UCRL- JC-104721
PREPRINT

HIGH-RESOLUTION ELECTRON MICROSCOPY OBSERVATIONS OF ATHERMAL OMEGA PHASE IN Ti-Mo ALLOYS

D. Schryvers
L.E. Tanner

This Paper was Prepared for Submittal to
Proceedings of the International Conference
on Martensite Transformations ICOMAT '89
Australian Institute of Metals
Sydney, Australia
July 3-7, 1989

June 26, 1990

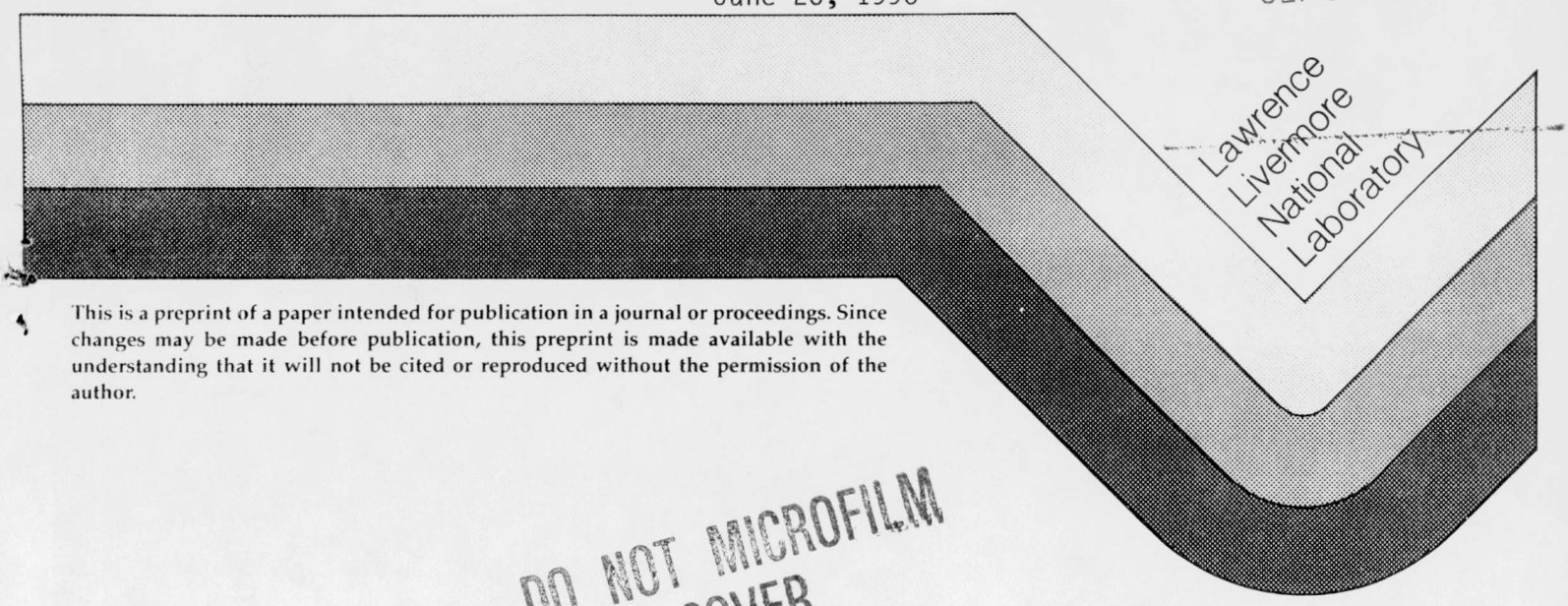

HIGH-RESOLUTION ELECTRON MICROSCOPY OBSERVATIONS OF ATHERMAL OMEGA PHASE IN Ti-Mo ALLOYS

D. Schryvers (a) and L. E. Tanner (b)

UCRL-JC--104721

DE90 017526

(a)University of Antwerp, RUCA, Groenenborgerlaan 171, B-2020 Antwerp, BELGIUM

(b)Chemistry & Materials Science Dept., Lawrence Livermore National Laboratory, P.O. Box 808, Livermore, CA 94550, USA

ABSTRACT

The commensurate and incommensurate structural configurations underlying the diffuse scattering from athermal ω found in the as-quenched β phase of Ti with 8 and15 at.% Mo have been investigated by high-resolution electron microscopy. Image interperetations were based on a simulation code developed via observed images of the commensurate ω phase formed by annealing Ti-8 at.% Mo. Athermal ω is observed as linear structural arrays or "strings" of <1.5 nm length. When commensurate (in quenched Ti-8 at.% Mo), the strings are confined to <111> directions which are parallel to the longitudinal displacement wavevector associated with this phase transformation. However, when the athermal ω is incommensurate (in quenched Ti-15 at.% Mo), the strings tend to deviate from this direction. Atomic models for one- and two-dimensional transition structures are proposed.

1. INTRODUCTION

The formation of the ω phase in BCC metals and alloyed solid solutions has been studied in great detail for more than two decades [1]. However, there remain several critical questions regarding local atomic configurations and their changes in the very initial stages of this displacive transformation, i.e, when the parent phase, β, is quenched from elevated temperature, and during subsequent thermal treatments [2-6]. We have recently found that local displacive effects may be rather well elucidated by using high-resolution transmission electron microscopy (HREM) in conjunction with electron and neutron (elastic and inelastic) scattering, e.g., see the studies of premartensitic behavior in Ni-Al alloys [7]. This same approach is being applied to examinations of athermally and isothermally formed ω in the Ti-Mo and Zr-Nb systems. This report deals with our initial HREM observations of ω in BCC β solid solutions of Ti with 8 and 15 at.% Mo, hereafter identified as 8Mo and15Mo, respectively.

It is well known that the scattering from athermal ω is characterized by curved sheets of diffuse scattering (DS) that either pass through ω nodes, e.g., $(2\pi/3)S_{222}$ (where S_{222} is the vector of the BCC reciprocal lattice site 222) or are slightly displaced $S_{222} + \delta$ [1,8,9], where the displacement $|\delta|$ usually increases (at times discontinuously) with increasing solute content [4,6]. The former is indicative of the formation of a structurally commensurate "ideal ω" or ω(c), whereas the latter suggests that a modulated incommensurate structure, ω(i), is formed [1,2,4]. When the diffuse and Bragg scattering are combined in the phase contrast TEM imaging mode, local atomic detail can be revealed; such HREM images do indeed show some significant differences between the ω(c) and ω(i) structures. We have been able to interpret these microstructures in terms of recent models [1,2,10-12], but in order to do so properly, it was first necessary to develop an image simulation code based on fully formed ω(c). This microstructure was developed by low-temperature isothermal annealing of the low-solute alloy. In the following sections, we first describe the image simulation procedure, then proceed to analyze the athermal ω found in the two alloys.

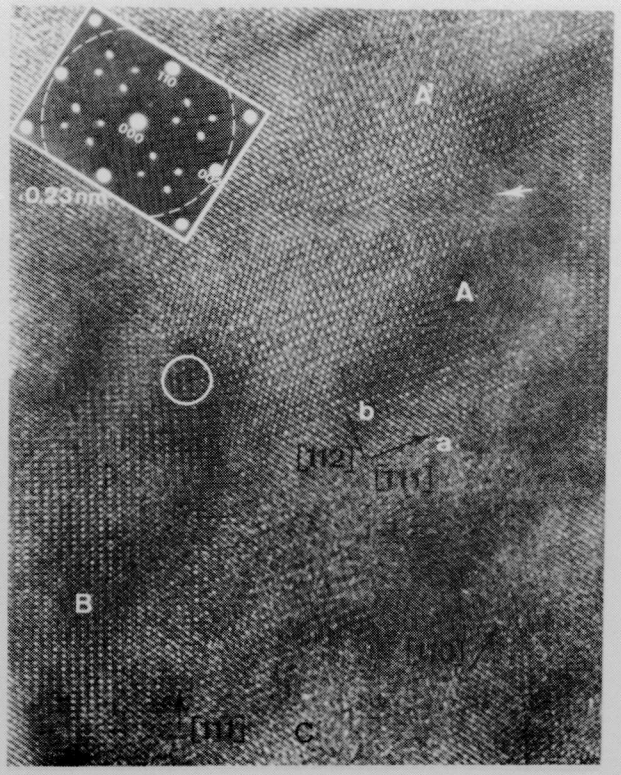

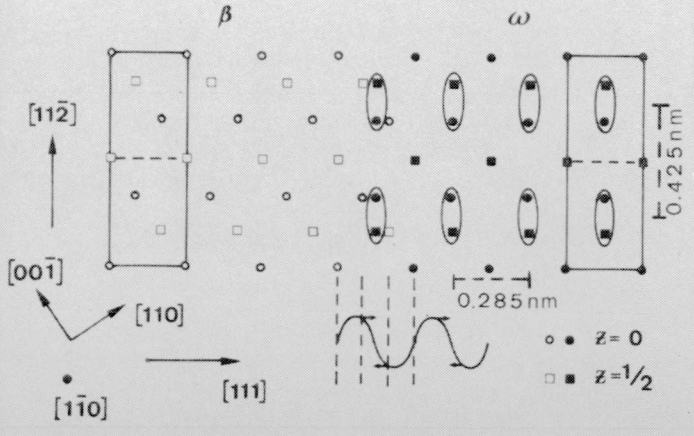

Figure 2. Schematic representation of the structural relationship between BCC β and ω as seen along the [1$\bar{1}$0] direction, including the longitudinal displacement wave.

Figure 1. HREM image of annealed 8Mo, including the properly oriented SAD pattern.

2. COMMENSURATE ω DOMAINS: THE HREM IMAGE SIMULATION CODE

Both alloys were water-quenched from 950 °C, and selected samples were held at 350 °C for periods of 10-200 h and followed by quenching. HREM examinations were made with a JEOL 4000EX instrument having an experimental resolution (i.e., at Scherzer defocus) of 0.17 nm. Selected-area diffraction (SAD) from 8Mo held for 100 h (inset, figure 1) shows that the diffuse scattering described earlier sharpens into discrete, but asymmetric, ω(c) reflections . The (1 $\bar{1}$0) HREM image in this figure (formed by using all the diffracted beams within the dotted circle that marks the size of the objective aperture) reveals elongated ω(c) domains of roughly 8 x 13 nm. Two of the four possible variants are in contrast, each containing a characteristic rectangular white dot pattern having a different orientation in each domain (marked A and B). The short dot spacing (0.285 nm) is along either [111] or [11$\bar{1}$], and the longer spacing (0.425 nm) is along [11$\bar{2}$] or [112], respectively. (Indices throughout refer to the basis BCC structure unless otherwise stated.) The smaller overall dimension of the domains is parallel to <112>, and this agrees with a shape factor elongation of ω reflections in the <112>* directions. Other portions of the image (marked C) show only (110) BCC lattice fringes. These regions are expected to contain the remaining two variants, which are out of contrast in this orientation. Indeed, when the sample is tilted through a sequence of zones containing the related reflections, we find that the images of these variants come into contrast appropriately and completely fill regions such as C. This leads to the conclusion that, at least at this stage of development, ω(c) domains of all four variants are contiguous throughout the bulk volume and, hence, apparently are <u>not</u> isolated particles in a β matrix as is so often described [1]. It is important to note that the ω white dots (e.g., in domain A) are located along extrapolations of the (110) fringes in an adjacent C-type region. The arrow in region A points towards an anti-phase boundary resulting from impingement of two domains of the same orientational variant but nucleated on differing subvariants [1,2]. The small circle indicates overlapping of the images of variants A and B.

The observed dot patterns are readily understood in terms of the structural change from β to fully developed ω(c). This transformation is facilitated by a longitudinal displacement modulation with wavevector $q=2/3(\pi/d)<111>$ of appropriate amplitude and phase, where d is the interplanar spacing [1,2]. This behavior is believed related to the anomalous dip in the LA[ζζζ] phonon branch at the same wavevector, viz. $\zeta = 2/3$ [2]. The resulting crystal structure is hexagonal according to the early analysis of Silcock [1]. The foregoing is schematically represented in the (1$\bar{1}$0) lattice projection in figure 2. Here we see that the stack of (111) planes undergoes a sequential displacement such that 2 out of 3 planes collapse towards each other, while the 3rd remains stationary, etc. The atoms in the collapsed planes (grouped within the ellipses as a schematic

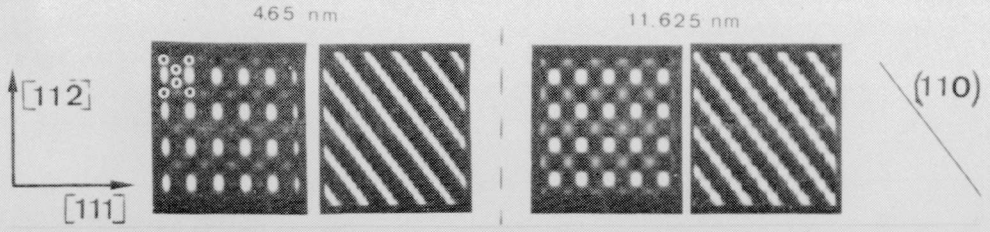

Figure 3. Selected computer simulated images for ω observed along β[1 $\bar{1}$0]. The position of the atom columns are indicated in the left-most ω image.

convenience) are rather closely spaced in projection, viz., ~0.13 nm, which is below the experimental resolution noted above. By assuming columns of these paired atoms through the foil thickness for imaging purposes, we find that they provide a rectangular array that corresponds to the observed dot pattern in both orientation and dimensions. We confirm this interpretation by using real-space methods for computer simulation of ω images in this orientation. Figure 3 shows examples selected with the same imaging conditions used for direct observation, together with the corresponding calculations for the untransformed β lattice (viz., {110} fringes). These images are typical for a wide range of defocus and thickness parameters and show that the rectangular array of white dots is the signature of ω; complete details of the simulations and interpretations will be published elsewhere [13]. It is further noted that, depending on the exact defocus and thickness values, the prominent white dots appear either at (Δf = -50 nm, t = 11.6 nm) or in between (Δf = -30 nm, t = 4.65 nm) the newly formed atom pairs. This is seen by comparing the positions of the white dots with the location of the input atomic configuration as indicated by small open circles in the upper left corner of figure 3. The white dots lie in (112) planes which contain the newly paired atoms (figure 2). Furthermore, the different positions of the ω white dots (as affected by varying imaging conditions) always coincide with the traces of the white (110) fringes in the corresponding calculated images of the β structure, and this also agrees with all our experimental observations.

3. TRANSITION MICROSTRUCTURES

3.1 The 8Mo Composition

Quenching 8Mo samples retains an early stage of the transition to the stucture described in Sec. 2. The SAD pattern (inset, figure 4) reveals peaks close to, but apparently not quite at commensurate positions $(2\pi/3)S_{222}$. In the HR image (figure 4), the line resolution of the (110) planes (viz., 0.23 nm) is clearly visible. Superimposed on this fringe pattern are local enhancements (dots) which group as linear arrays or "strings" generally lying along <111> directions. The strings thus group into two separate "variants", differing only in their orientation. Using the simulation code developed earlier, the string images may be interpreted in the simplest sense as one-dimensional modulations corresponding to the displacement wave shown in figure 2. However, when examining various groupings of adjacent strings, it can be seen that the ω correlations perpendicular to the modulation wave are increasing as well (see arrows), although they remain substantially smaller than those parallel to the wavevector. This transition to higher dimensionality and perfection can be directly related to the emerging commensurate diffraction peaks. Anti-phase correlations between certain adjacent strings can also be seen (see arrows).

3.2 The 15Mo Composition

A similar, but less developed, microstructure is found in as-quenched 15Mo. However, unlike 8Mo, this microstructure shows little or no change with subsequent annealing for up to 200 h at 350 °C. The as-quenched SAD pattern (inset, figure 5) is characteristic of ω(i) displaying only DS arcs which, for this higher solute content, are displaced by $\delta \approx 0.06$ from commensurate positions (the latter marked by crosses). The linear dot pattern in the HREM image (figure 5) is primarily one-dimensional in this case, i.e., there is rather little correlation normal to the modulation wavevector. Digital Fourier analysis followed by back image processing unambiguously relates the DS to the local atomic configurations [13]. However, when the dot locations and the orientations of the strings are compared with the (110) fringes in both direct and processed images, we find that the orientations invariably deviate from <111> by as much as a 10° rotatation towards (never away from) [110]. This proves to be a most significant observation with respect to the modulated ω(i) structure and will be discussed in Section 4.

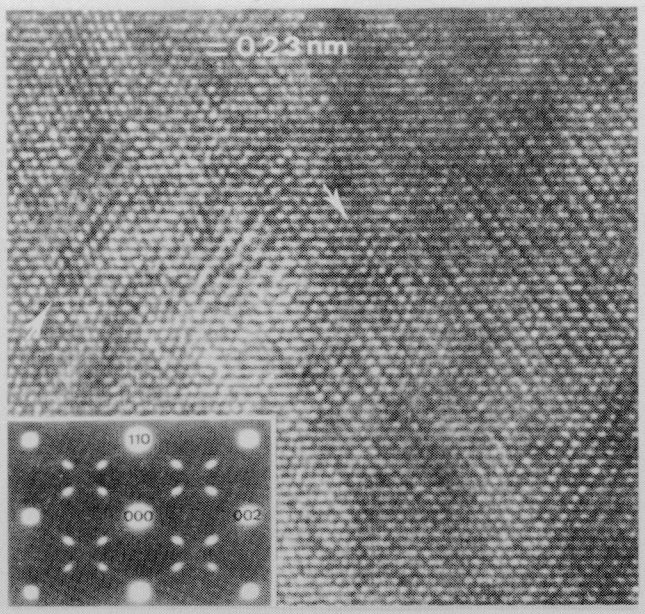

Figure 4. The [1 $\bar{1}$0]. HREM image of as-quenched 8Mo revealing small, nearly commensurate one- and two-dimensional ω regions.

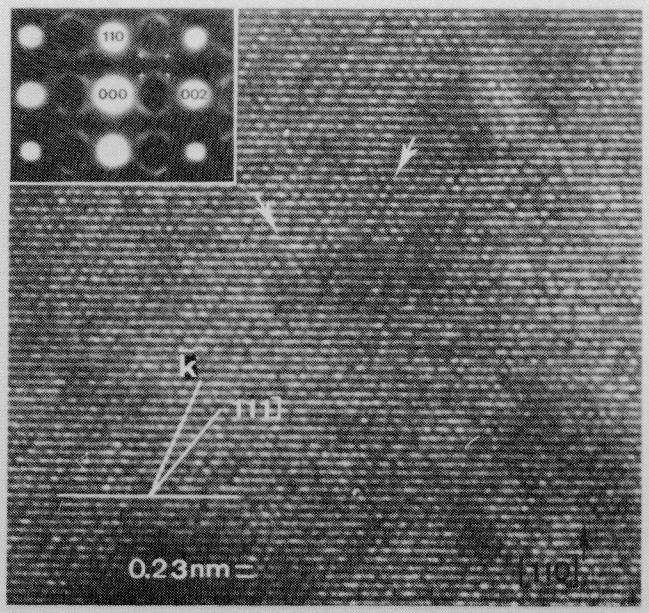

Figure 5. The [1$\bar{1}$0] HREM image of as-quenched 15Mo showing ω(i), viz., short strings of white dots superimposed on the BCC (110) lattice fringes.

4. DISCUSSION

Using the structural signature for three-dimensional ω(c), we have identifed athermal ω in quenched 8Mo as an interwoven assembly of small (<1.5 nm length) one- and two-dimensional linear atomic arrays (strings) generally aligned along <111>. In quenched 15Mo, however, the athermal ω strings, which are invariably one-dimensional, often deviate by as much as 10° from the <111> displacement wave direction. Each <111> row of n white dots represents the collapse of 2n atoms, i.e., only one row of projected atom pairs as shown schematically in figure 7a. We can calculate the image of such a single string of ω(c) embedded at some depth in the foil surrounded by otherwise unperturbed β (see figure 6). The result is a local contrast enhancement of adjacent (110) fringes which align along [111] as shown in figure 8a. The development of two-dimensional correlations (i.e., normal to the displacement wavevector) involves coalesence of adjacent strings in-phase giving rise to the rectangular ω pattern already described (figure 2). A thickening of the string in depth (i.e., along the incident beam direction [110]) increases the dot brightness [13]. The model for adjacent ω(c) strings of the same variant in anti-phase juxtaposition is shown in figure 7b with the corresponding calculated image in figure 8b.

We now address what we believe to be the characteristic image of the ω(i) string images. The observed deviation from <111> is incorporated into our model (figure 7c) by shifting the collapsing atoms to successive (112) planes, namely a phase slip of $+2\pi/3$. The calculated image of this stepped array is shown in figure 8c and agrees rather well with our observations. Therefore, for these experimental conditions and resolution, the array of dots is found to deviate from the actual displacement wavevector direction and follows the average alignment of the imposed structural "steps" (where the number of steps per unit length determines the angle of deviation). Such a series of phase slips corresponds with the soliton or discommensuration models of ω(i) proposed recently by several authors [10-12], although they did not deal with the specific details of the configuration, e.g., the possibility of such a jogged or stepped array, the degree of correlation normal to the displacement wavevector, etc. According to this description, the $+2\pi/3$ shift produces a local collapse of the lattice between sections of otherwise perfect ω(c), and this correctly accounts for the observed displacement of the DS [12]. In this context, it is important to note that a deviation away from [110], which was never observed, would require a phase slip of $-2\pi/3$ and this is energetically unfavorable since it leads to incompatable configurations, i.e.,"anti-ω" [11,12]. Another linear defect model was proposed by Sanchez and deFontaine [2] involving a sinusoidal displacement field related to a complex assembly of subvariants. Our observations do not confirm the details of this arrangement, which in fact involve more extensive correlations normal to <111> than are revealed in the images.

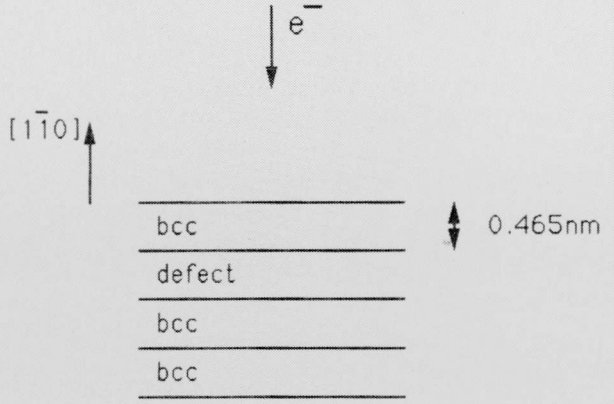

Figure 6. Schematic of linear ω defects embedded in a thin foil between undeformed BCC (as seen along the electron beam direction).

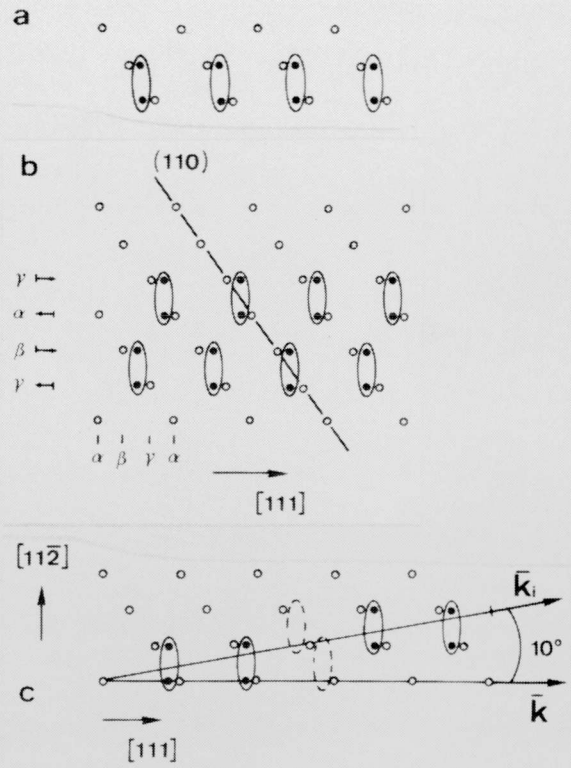

Figure 7. Atomic models proposed for (a) a single commensurate ω modulation along <111>, (b) a two-dimensional ω modulation in anti-phase juxtaposition and (c) a single modulation including an angular deviation of 10°, viz., incommensurate ω.

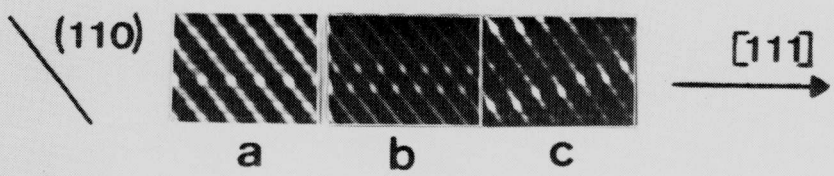

Figure 8. Computer simulations of the models in figures 7a, b & c, respectively; positioned as shown in figure 6 and given for a total thickness of 2.69 nm at Δf =-50 nm.

The only other HREM studies to date that we are aware of were carried out by Hida et al. [14]. They proposed several interesting atomic configurations for transitional states synthesized from detailed information obtained by x-ray and electron scattering, EXAFS, as well as TEM, in both amplitude and phase contrast imaging modes. Of these models, the closest to our HREM observations is a needle-shaped structure whose axis is along [111] (see figure 11e, Ref.[14b]). It is constructed by stacking a series of chain-like [11$\bar{2}$] atomic configurations , each lying in successive (111) planes. This has similarities to our model (figure 7a), but , as with the Sanchez and deFontaine model [2], the [11$\bar{2}$] correlations extend too far when compared to our HREM images of 15Mo. That is, our computer simulations prove that each white dot corresponds with just a single pair of collapsed atoms. Hence, the Hida et al. model would require double strings of white dots where only single strings are observed. Furthermore, none of the models presented by the Hida group [14b] directly address the atomic configurations that might lead to an incommensurate structure, nor did they report on any directional deviation of the defect strings in their HREM images of as-quenched structures.

We are continuing to investigate the early and later stages of the transformation in this and the Zr-Nb alloy system. Correlations will be made with elastic and inelastic neutron scattering observations [15]. Our purpose is to (a) elucidate the displacive relaxation sequence from one- to three-dimensional ω, (b) determine the configurational details ω(i) → ω(c), (c) identify when chemical changes occur that convert the apparent single-

phase domain structure of ω to a metastable two-phase assembly of solute-lean ω plus solute-enriched β and subsequently, to an equilibrium α+β microstructure. Ultimately, this will lead to a definative understanding of the stable and metastable phase relations in these families of alloy systems [16], and in particular, what role the β phase separation may play regarding the development of incommensurate ω structures [2,17].

5. CONCLUSIONS

Using HREM, we have identified the local configurations related to the linear defect structure of athermal ω. These string-like arrangements (<1.5 nm in length) are confined to <111> when commensurate, but deviate by as much as 10° toward <110> when incommensurate. The latter can be modeled in terms of a linear ω(c) array jogged by $+2\pi/3$ phase slips and is confirmed by appropriate image simulations. This description is in keeping with several theoretical models involving soliton concepts [10-12].
In the present paper the emphasis is on the interpretation of HREM images of different stages of the BCC → ω transformation process. Starting with the presently accepted model for the ω structure and its relation to the HR images, i.e., creating an image simulation code, possible constructions of the atomic configurations for the transition or precursor states are presented. It is clear that the information on the exact atom positions as distilled from HREM images and corresponding computer simulations is limited. However, the direct nature of these images proves to be of great importance for the detection of local deviations from otherwise averaged information as obtained previously by a variety of other techniques [1].

ACKNOWLEDGEMENTS

The authors wish to thank the National Center for Electron Microscopy at the Lawrence Berkeley Laboratory for the use of their facilities. This work was performed under the auspices of the U. S. Department of Energy by the Lawrence Livermore National Laboratory under Contract No. W-7405-ENG-48.

REFERENCES

1. Sikka, S. K., Vohra, Y and Chidambaram, R.: Prog. Mat. Sci., 1982, 27, 245.
2. deFontaine, D.: Met Trans. A, 1988, 19A, 169.
3. Tanner, L. E.: Competing Interactions and Microstructures, Springer Proc. in Physics, (R. LeSar, A. Bishop and R. Heffner, eds.), Vol. 27, (Springer-Verlag, Berlin) 1988, p. 74.
4. Vlasova, Ye.S., D'Yakanova, N. B. and Lyasotskiy, I. V.: Phys. Met. Metall., 1984, 57, No. 3, 167.
5. Lyasotskiy, I. V. and D'Yakonova, N. B.: Phys. Met. Metall., 1980, 50, No.1, 118.
6. Terauchi, H., Sakaue, K., and Hida, M.: J. Phys. Soc. Japan, 1981, 50, 3932.
7. Schryvers, D., Tanner, L. E. and Shapiro, S. M.: Shape Memory Materials, Int. Mtgs. on Adv. Mtls., (K. Otsuka and K. Shimizu, eds.), Vol. 9, (M.R.S., Pittsburgh), 1989, p.35.
8. deFontaine, D., Paton, N. E. and Williams, J. C.: Acta Metall.,1971, 19, 1153.
9. Lyasotskiy, I. V. and Tyapkin, Yu. D.: Phys. Met. Metall., 1973, 36, No. 6, 1260.
10. Borie, B., Sass, S. L. and Andreassen, A.: Acta Cryst., 1973, A29, 585, 594.
11. Pynn, R.: J. Phys. F, 1978, 8, 1.
12. Horovitz, B., Murray, J. L. and Krumhansl, J. A.: Phys. Rev. B, 1978, 18, 3549.
13. Schryvers, D. and Tanner, L. E.: to be published.
14. (a) Sukedai, E , Hashimoto, H. and Hida, M.: Jpn. J. Appl. Phys., 1987, 26, L961;
    (b) Hida, M., Sukeda, E.and Terauchi, H.: Acta Metall., 1988, 36,1429.
15. Shapiro, S. M., Larese, J. Z., Noda, Y. and Yamada, Y.: research in progress.
16. Moffat, D. L. and Kattner, U. R.: Met. Trans. A.,19A, 2389.
17. Hayman, C.: unpublished.

Technical Information Department · Lawrence Livermore National Laboratory
University of California · Livermore, California 94551